Computational Materials Science 48 (2010) 267–281

Contents lists available at ScienceDirect

Computational Materials Science

journal homepage: www.elsevier.com/locate/commatsci

A 3D Monte Carlo study of the effect of grain boundary anisotropy and particles on the size distribution of grains after recrystallisation and grain growth

Egil Fjeldberg, Knut Marthinsen *

Department of Materials Science and Engineering, Norwegian University of Science and Technology, N-7491 Trondheim, Norway

ARTICLE INFO

Article history:
Received 29 June 2009
Received in revised form 23 December 2009
Accepted 14 January 2010
Available online 16 February 2010

Keywords:
Computer simulation
Potts Monte Carlo
Grain growth
Recrystallisation
Grain size distribution
Grain boundary anisotropy
Particle effects

ABSTRACT

The present paper considers 3D grain size distributions and how they evolve during and after recrystallisation and grain growth as investigated by a 3D Potts Monte Carlo (MC) model. Two particular cases have been studied: (i) the effects of anisotropy in grain boundary energy and boundary mobility on grain size distributions after recrystallisation and (ii) the effects of second phase particles on the size distributions after both recrystallisation and grain growth. The present 3D MC simulations have shown that anisotropy has a strong effect on the size distributions of grains after recrystallisation, however, mainly in terms of a large and increasing fraction of small grains with increasing anisotropy. After "correcting" for the unrealistic large number of small grains, the differences between the different cases become quite small, but based on an evaluation of the skewness in these "corrected" grain size distributions, a small shift from a normal towards a log-normal-like distribution is still indicated. Concerning the effect of particles, simulations have shown that for an increasing volume fraction of particles, the coarsened microstructures show a clear shift from a Gaussian like towards a log-normal-like distribution. This behaviour is observed both for grain growth alone and for recrystallisation and subsequent coarsening.

1. Introduction

Recrystallisation and grain growth are the key microstructural process to control grain size and texture during thermo-mechanical processing of metals and alloys, which again determine properties like strength, fatigue and formability. However, although recrystallisation and grain growth have been subject of extensive investigations, both experimentally and theoretically, during many decades, there are still important aspects which are not fully understood.

A common and still intriguing problem which is observed in relation to computer simulations of both recrystallisation and grain growth and precipitation as well, is that the predicted size distributions of grains (during recrystallisation and grain growth) and of precipitates (during nucleation, growth and coarsening) in most cases do not reproduce what is observed experimentally. In the latter case of precipitation/coarsening, simulations typically give a LSW (Lifshitz, Slyszov and Wagner) distribution [1,2], which is far from the log-normal distribution typically observed experimentally [3,4]. After recrystallisation and during grain growth a log-normal size distribution of grains is commonly observed irrespective of material and processing conditions, while most models and computer simulations typically predicts a more left-skewed distribution on a logarithmic scale [5,6], i.e. the tail on the left-hand side is longer than that on the right-hand side.

This discrepancy is a problem of fundamental interest, and it relates to the reliability of the computer simulation models when it comes to comparison with experiments. The problem has occasionally been addressed and discussed in the literature, and although previous work has indicated that it is most probably related to deviations from idealised conditions such as random distribution of nuclei and homogeneous and constant growth, this is still an aspect of debate and not fully understood, see e.g. [5–7].

In the present work we have investigated grain size distributions by means of 3D Monte Carlo simulations in two particular cases. In the first case the effects of anisotropy, i.e. a misorientation-dependent grain boundary energy (GBE) and grain boundary mobility, on the grain size distribution after recrystallisation, have been investigated. These simulations are based on a standard 3D MC code (including anisotropy in grain boundary energy and mobility; for details see below) for grain growth and recrystallisation run on a serial computer (see e.g. [8–10] for excellent reviews and references). In the present work, only site saturated, spatially random nucleation is considered, a condition which may be considered to mimic particle stimulated nucleation (PSN) of recrystallisation, which e.g. is the dominant nucleation mechanism in many aluminium alloys.

In the second case anisotropy is neglected and the effect of second phase particles on the grain size distribution during

* Corresponding author. Tel.: +47 73 59 34 73; fax: +47 73 55 02 03.
E-mail address: knut.marthinsen@material.ntnu.no (K. Marthinsen).

0927-0256/$ - see front matter © 2010 Elsevier B.V. All rights reserved.
doi:10.1016/j.commatsci.2010.01.007

recrystallisation and during subsequent coarsening/grain growth has been emphasised. As the inclusion of particles requires a much larger MC lattice [11], which is quite demanding in terms of computer power and memory, these simulations are based on the use of a 3D parallel MC code. The results for the two cases considered are presented in Sections 3 and 4, respectively.

It should be mentioned that some preliminary results of the present work already has been presented elsewhere [12].

2. Simulation method

In both cases presented below basically the same basic simulation code is used. The general simulation method is therefore presented here.

First a microstructure is mapped onto a 3D lattice where each lattice site is assigned a number S_i, which has a value between 1 and Q. S_i corresponds to the orientation of the grain, Q is the total number of orientations, and all neighbouring lattice sites with the same orientation are regarded as being within the same grain, while neighbouring lattice sites with another orientation are regarded as being part of another grain, and these grains are separated by a grain boundary. Each unlike pair of neighbouring orientations contributes with a grain boundary energy, $\gamma(S_i, S_j)$, to the total system energy. In addition each site also contribute with a stored energy, $H(S_i)$, to the total system energy, where $H(S_i) = 0$ for recrystallised grains and $H(S_i)$ is constant for deformed grains. This gives a total system energy, E, defined by

$$E = \frac{1}{2}\sum_{i=1}^{N}\sum_{j=1}^{nn}\left(\gamma(S_i, S_j)(1-\delta_{S_iS_j})\right) + \sum_{i=1}^{N} H(S_i) \tag{1}$$

where the sum, on i, is taken over all lattice sites, N, and the inner sum is taken over the nn nearest neighbours (equal to 26 in a simple cubic three dimensional lattice) of site i.

The evolution of the microstructure is modelled by picking a site i at random and calculating the energy change, ΔE which is associated with changing the spin of site i from S_i to S_i'. This reorientation is accepted with a probability p calculated from

$$p(S_i, S_j, \Delta E) = \begin{cases} \frac{\gamma(S_i,S_j)}{\gamma_m}\frac{M(S_i,S_j)}{M_m} & \text{if} \quad \Delta E \leqslant 0 \\ \frac{\gamma(S_i,S_j)}{\gamma_m}\frac{M(S_i,S_j)}{M_m}\exp\left(-\frac{\Delta E}{kT\gamma(S_i,S_j)}\right) & \text{if} \quad \Delta E > 0 \end{cases} \tag{2}$$

where $\gamma(S_i, S_j)$ and $M(S_i, S_j)$ are the grain boundary energy and mobility, respectively, between grains of spin S_i and S_j while γ_m and M_m are the maximum grain boundary energy and mobility. k is the Boltzman constant and T is the temperature.

In the case of no anisotropy the grain boundary energy function and the boundary mobility function in Eq. (2) are taken to be constant, i.e. independent of misorientation.

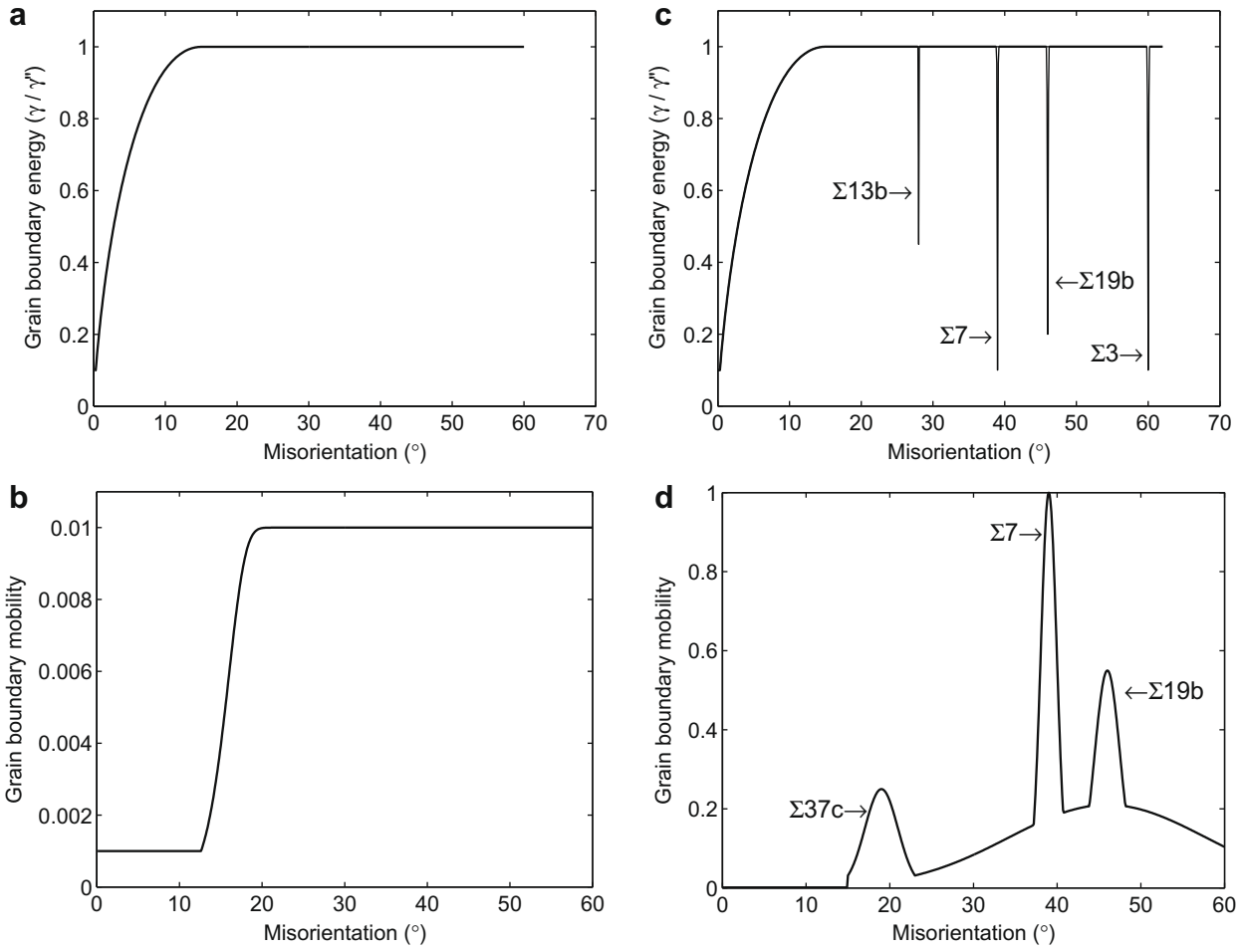

Fig. 1. The anisotropic grain boundary energy and mobility functions, where the Σ-boundaries correspond to rotations about the 111-axis. (a) The Read–Shockley grain boundary energy function. (b) The stepped grain boundary mobility function. (c) The anisotropic grain boundary energy function, including special boundaries. (d) The anisotropic grain boundary mobility function, including special high mobility boundaries.

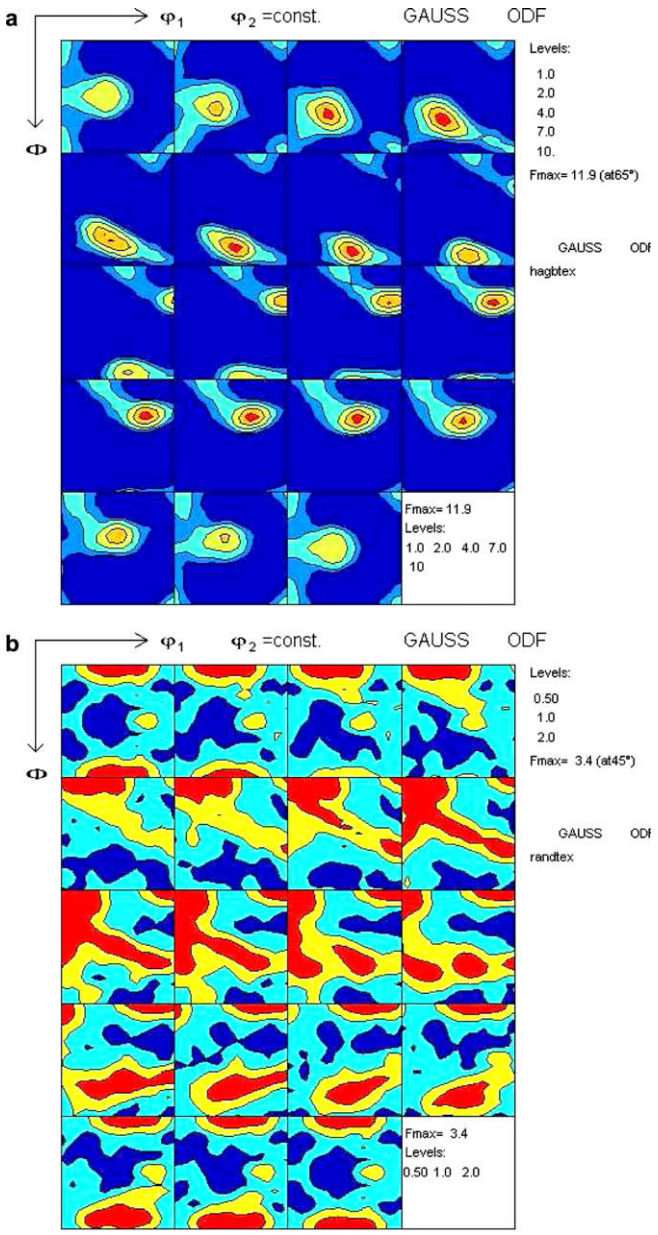

Fig. 2. Orientation Distribution Functions (ODFs) illustrating the deformation texture (a) and the PSN nucleation texture (b) used as input in the simulations.

3. Effect of anisotropy on the grain size distribution

3.1. Simulation setup

In this part of the work a standard 3D Potts Monte Carlo model [8,10], including anisotropy in grain boundary energy and grain boundary mobility (dependent on misorientation) has been used, and a systematic study of the effect of the different anisotropy factors on the growth kinetics and size distribution of the recrystallised grains has been carried out.

The first attempts to include anisotropic grain properties into Potts MC model simulations dates back to the eighties (e.g. [13,14]). The more generalised approach used in the present simulations, as described in Section 2, with an anisotropic grain boundary energy, $\gamma(S_i, S_j)$, and an anisotropic grain boundary mobility, $M(S_i, S_j)$, and with a switching probablity as given by Eq. (2), goes back to Holm et al. [15]. Recently this approach was further generalised to also include the grain boundary characteristics of certain special boundaries, so-called coincident site lattices (CSLs) [16–17]. The grain boundaries are divided into low angle grain boundaries, LAGB, (misorientation $\theta \leqslant 15°$) and high angle grain boundaries, HAGB, (misorientation $\theta > 15°$). In the low misorientation regime the energy is expressed by the Read–Shockley (RS) equation, see Eq. (3), where θ_m is the misorientation at which the boundary becomes a high angle boundary (typically $\theta_m = 15°$)

$$\gamma = \gamma_m \frac{\theta}{\theta_m}\left(1 - \ln\left(\frac{\theta}{\theta_m}\right)\right) \tag{3}$$

The HAGB energy is a constant equal to γ_m (γ; Fig. 1a), except for certain "special" boundaries corresponding to particular misorientation angles (coincidence site lattices, CSLs). The special boundaries accounted for in the present simulations are of the $\Sigma 3$, $\Sigma 7$, $\Sigma 13b$ and $\Sigma 19b$ types which are represented as sharp minima (cusps) in the Read–Shockley energy function (see Fig. 1c) [16,17]. Just as the grain boundary energy, the grain boundary mobility is also dependent on the grain boundary misorientation. In the simplest case the mobility function is a step function (Fig. 1b), where the mobility equals 0.001 when the misorientation is below θ_m (LAGBs) and, except for the special boundaries, equals 0.01 when $\theta > \theta_m$, i.e. for the HAGBs. The special mobility boundaries considered are at $\Sigma 7$, $\Sigma 19b$ and $\Sigma 37c$ (Fig. 1d) with distinct peaks in the mobility function at these special boundaries [16,17]. The initial size and width of these peaks and minima used in the present work are identical to the ones which have been fitted to mimic the experimental texture evolution of a deformed commercial purity aluminium alloy, i.e. an AA1050 alloy [17,18].

Together with the computational aspects discussed above, the *n*-fold Way approach [19] is used to speed up the simulations. In all cases the same initial microstructure is used. The simulation system is a cubical box of 100^3 lattice sites (voxels) with periodic boundary conditions. This is a fairly small system, however, a sub-set of simulations run with a system size of $200 \times 200 \times 200$ lattice sites (see also Section 5), indicate that this is not critical for the present results. The initial microstructure consists of 823 nearly equiaxed grains constructed by a Voronoi tesselation of space from a set of randomly distributed points, by means of the so-called Microstructure Builder, the details of which are described elsewhere [17,20]. 16,500 nuclei are added at time zero, where each nucleus has a size of 3 lattice sites, i.e. corresponding to 5 vol.% nuclei and site saturation nucleation. A value of 0.9 has been used for the simulation "temperature" (kT), in accordance with the recommendations in [16]. A limited sensitivity analysis to this parameter have been performed (see Section 5), which indicates that a simulation temperature of 0.9 is an adequate value and that the present results are not critically sensitive to this parameter. The initial texture used corresponds to the deformation texture at the transfer gauge of industrial rolling of an Al–Mg–Mn-alloy (AA3103) [21], see Fig. 2a. The texture is included by discretising the Orientation Distribution Function (ODF) of the actual deformation texture, in terms of individual Euler angles, which were then assigned randomly to the initial 823 grains, corresponding to a so-called statistical (random) misorientation distribution function [22]. Assuming PSN to be the dominating nucleation mechanism, a quite weak, but not fully random PSN-texture is used for the nucleation spectrum, see Fig. 2b. This nucleation texture is calculated from a recrystallisation texture model due to Engler [23], where only the deformation texture is taken as input.

Seven different cases have been investigated, involving various combinations of the different forms of anisotropy in the grain boundary energy and grain boundary mobility functions:

1. *Fully isotropic system*: Constant grain boundary mobility and grain boundary energy.
2. *Isotropic GBE, step mobility*: Constant grain boundary energy (GBE) and a stepped grain boundary mobility function, cf. Fig. 1b.

Table 1
A selection of relevant simulation parameters and results for the different simulation cases. All results are averaged over 10 runs. RS = Read–Shockley, GBE = grain boundary energy, mob = mobility and aniso = anisotropic.

Case	Type of GBE and mob	# grains	Time ~100% RX (MCS)	Number of grains $V \leqslant 3$	Avrami exponent
1	Full isotropy, mob = 1	5425	2×10^4	$\frac{309}{5425} = 5.8\%$	3.0 (at t_0 = 3000 MCS)
2	Isotropic GBE, step mob	5603	2×10^6	$\frac{413}{5603} = 7.4\%$	
3	RS GBE, isotropic mob	5505	2×10^6	$\frac{508}{5505} = 9.2\%$	
4	RS GBE and step mob	5910	2×10^6	$\frac{716}{5901} = 12.1\%$	
5	Aniso GBE, step mob	4767	3×10^6	$\frac{836}{4767} = 17.5\%$	
6	RS GBE, aniso mob	6924	2×10^5	$\frac{1829}{6924} = 26.4\%$	
7	Full (original) anisotropy	6121	3×10^5	$\frac{1900}{6121} = 31.0\%$	3.0 (at t_0 = 27,000 MCS)

3. *RS GBE, isotropic mobility*: Read–Shockley grain boundary energy and constant grain boundary mobility, cf. Fig. 1a.
4. *RS GBE, step mobility*: A Read–Shockley grain boundary energy and a stepped grain boundary mobility function, cf. Fig. 1a and b.
5. *Anisotropic GBE, step mobility*: A fully anisotropic grain boundary energy and a stepped grain boundary mobility function, cf. Fig. 1b and c.
6. *RS GBE, anisotropic mobility*: A Read–Shockley grain boundary energy and a fully anisotropic grain boundary mobility, cf. Fig. 1a and d.
7. *Fully anisotropic system*: Both a fully anisotropic mobility and a fully anisotropic grain boundary energy, cf. Fig. 1d and c.

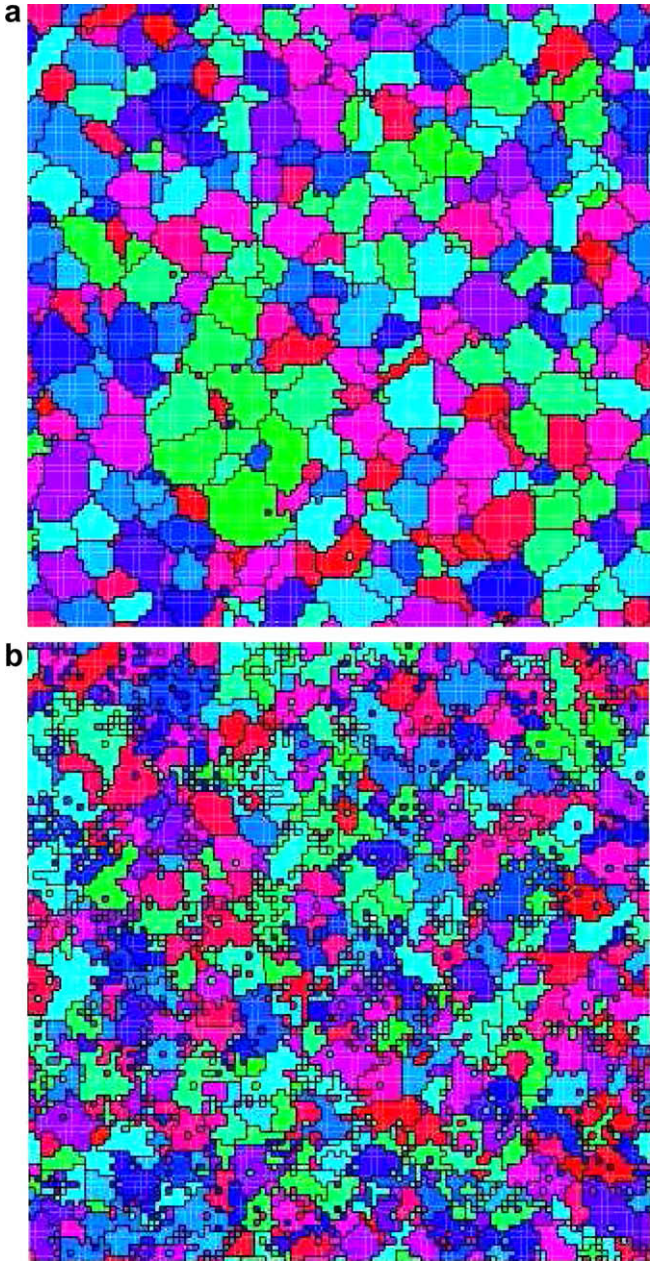

Fig. 3. 2D sections of simulated microstructures corresponding to ~100% recrystallisation. (a) The microstructure for the isotropic case, Case 1. (b) The microstructure for the anisotropic case, Case 7.

3.2. Results and discussion

Table 1 summarises some key parameters for the different simulation cases. All data are for approximate 100% recrystallisation (i.e. $X(t) \sim 1$) and the results are averaged over 10 runs.

From Table 1 one notices that the time, t, to reach 100% recrystallisation varies quite much. However, as far as the Avrami exponent is concerned, i.e. the time exponent, n, of the classical JMAK equation $X(t) = 1 - \exp(-kt^n)$, see e.g. [24], the anisotropy introduced through a misorientation-dependent grain boundary energy and boundary mobility has no effect. This is exemplified in Table 1 for the two "extreme" cases, no anisotropy and a fully anisotropic system. Except for an initial transient which is quite different in the two cases and whose effect on the Avrami exponent can be eliminated by introducing a transient time t_0 in the JMAK equation [25,26], both cases are well represented by an exponent of $n = 3$, in agreement with the theoretical value corresponding to site saturation nucleation and homogeneous, constant growth. This means that although the anisotropic grain boundary energy and mobility functions introduce variations in the growth behaviour, these are local effects in space and time and do not affect the overall average kinetics behaviour. The reason for the difference in time it takes to reach a 100% recrystallised microstructure relates to the calcula-

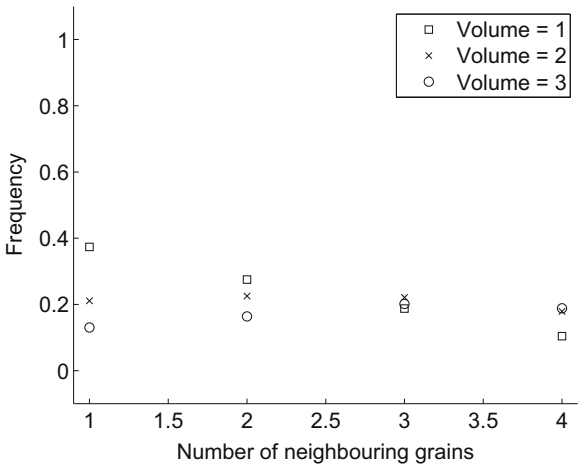

Fig. 4. A graph showing the number of neighbours to the small grains left in the microstructure in the fully anisotropic case, Case 7.

tion of the time increment, Δt, after each flip of a lattice point in the microstructure:

$$\Delta t \sim -\frac{1}{A} \times \ln R \tag{4}$$

where R is a random number between 0 and 1 and A is the sum over all probabilities $p(S_i, S_j, \Delta E)$, see Eq. (2). When the grain boundary energy and mobility change, also $p(S_i, S_j, \Delta E)$ in Eq. (2) and correspondingly the A-value in Eq. (4) changes, which again affects Δt. In Case 1 is e.g. the mobility = 1, while the maximum mobility in both Cases 2 and 3 is 0.01. This corresponds to a factor of 100 between the mobilities, which quite accurately corresponds to the time difference to reach ~100% recrystallisation in these cases.

The most striking variation in Table 1 is related to the number of small grains which increases significantly with increasing degree of anisotropy (in Table 1 exemplified by # grains $V \leqslant 3$ voxels). The higher the anisotropy is, the more grain boundaries with a low energy there are, i.e. a large fraction of relative stable grain boundary segments. This aspect is illustrated in Fig. 3, showing a 2D picture of the microstructure at ~100% recrystallisation for Case 1, Fig. 3a (fully isotropic) and Case 7, Fig. 3b (fully anisotropic). One clearly sees a large increase in the number of small grains from the isotropic to the anisotropic case. An analysis of the number of neighbours to the small grains ($V \leqslant 3$) in the fully anisotropic case, Case 7, has also been made, see Fig. 4. As seen, a large fraction of the small grains are surrounded by few grains, and around 35% of the grains consisting of one lattice site is island grains, i.e. grains surrounded by only one large grain. This result originates from the anisotropy; grain boundaries with a low misorientation become stable/less mobile, due to both low grain boundary energy and low boundary mobility, resulting in quite stable, small grains.

Although the number fraction of small grains is quite large, it represents a very small volume fraction. Nevertheless, as will be further discussed below, this phenomenon complicates the comparison of the grain size distributions for the different cases. First

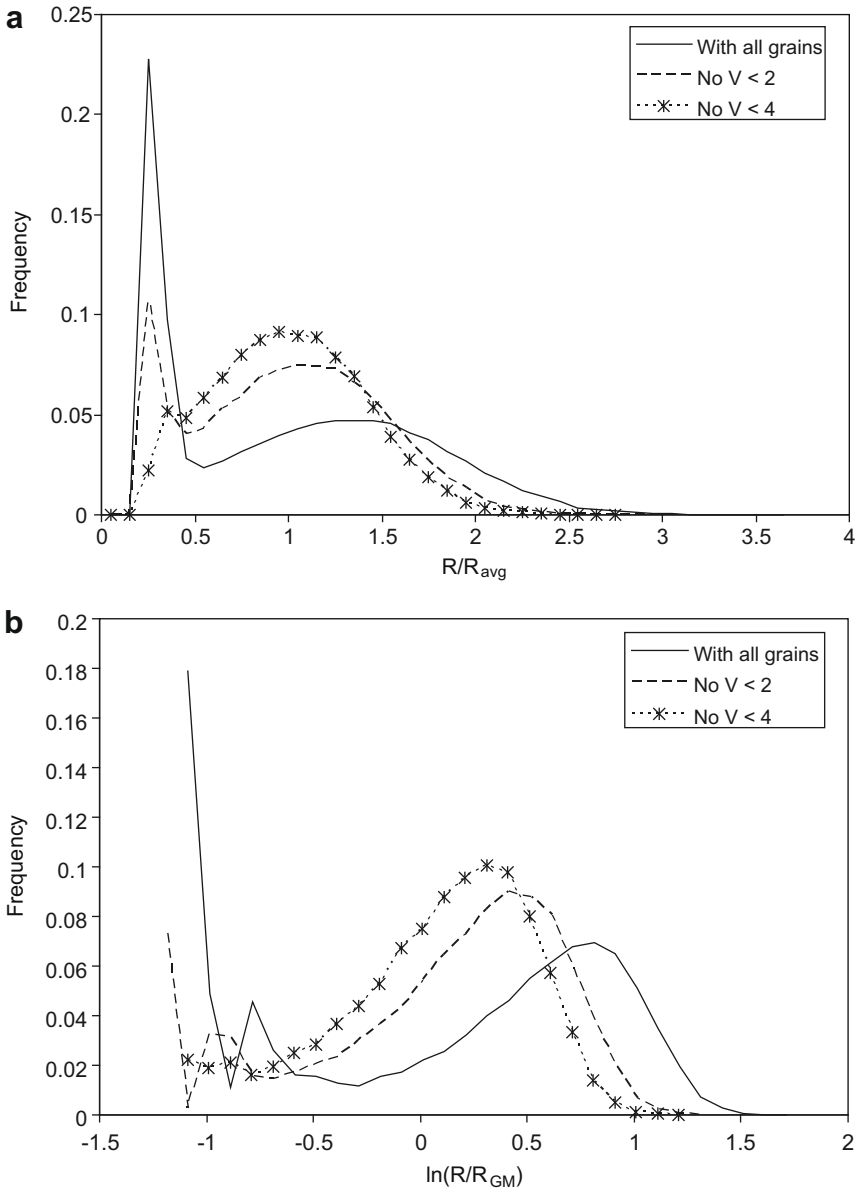

Fig. 5. Graphs showing the grain size distributions for a simulation run with the grain boundary energy in Fig. 1c and the mobility function in Fig. 1d, i.e. Case 7, comparing the case with all grains (as simulated) and the resulting size distributions when grains with volumes $V \leqslant 1$ lattice sites and $V \leqslant 3$ lattice sites, respectively, are removed. (a) The size distributions on a linear scale. (b) The size distributions on a logarithmic scale.

of all, the large amount of small grains makes is difficult to make a simple and direct comparison between the different grain size distributions. Therefore the effect of removing the smallest grains has been tested out, illustrated here for the case of full anisotropy, Case 7, Fig. 5a and b, which show the grain size distributions on a linear and on a logarithmic scale, respectively. While R_{avg} is the standard arithmetic mean the data presented on a logarithmic scale uses a grain size distribution which is normalised with the geometrical mean, R_{GM}, as calculated from [5]:

$$\ln(R_{GM}) = \frac{1}{N}\sum_i \ln(R_i) \tag{5}$$

where N is the total number of grains in the system and R_i is the size of grain i, calculated from the cubic root of the grain volume, i.e. assuming for simplicity all grains to have a cubical shape.

Fig. 5 shows the original grain size distributions (as simulated) and the distribution where grains with volumes of 1 and 3 lattice sites, respectively, have been removed.

Only a very small fraction of the small grains which are removed are old, deformed grains, and the majority of these are neighbours to only one grain, probably with approximately the same texture. The rest of the small grains are recrystallised grains either positioned inside one grain (island grains) or positioned on a grain boundary between two or more grains, probably an immobile grain boundary due to low grain boundary energy.

As illustrated in Fig. 5, the peak corresponding to the smallest grains is removed by introducing a cutoff. However, the size distributions get a rather strange unphysical shape at small grains, which is probably a poor representation of real microstructures. Therefore another way of overcoming the problem with small grains has also been introduced, viz. a manual "best fit" extrapolation when approaching $R/R_{avg} = 0$, i.e. in the region of small grains.

Fig. 6 illustrates as an example how these two ways of handling the small grain problem changes the grain size distribution. Fig. 6 shows the grain size distribution for the fully isotropic system, Case 1, and the fully anisotropic system, Case 7. Referring to the two original size distributions we see that they are quite different. The fully isotropic distribution (solid line) is, except for a small peak at small grains, close to a Gaussian (or normal) distribution. The size distribution for the fully anisotropic system is more difficult to characterise, mainly due to the large fraction of small grains which show up as a rather large peak for small grains, completely dominating the distribution. In an attempt to do reasonable comparisons between the different cases two more graphs are added, viz. one where all grains with volume less than four voxels ($V \leqslant 3$) are removed and a second where a large amount of the small grains are manually removed to make the left end of the graph as smooth as possible through extrapolation. However, direct comparisons are still difficult and a more quantitative measure is needed. One way to quantify how close a distribution is to a normal or Gauss distribution is to calculate the skewness, γ_1, which is a measure of the asymmetry of the distribution. The skewness, also known as the 3rd momentum [27], is defined as

$$\gamma_1 = \frac{\frac{1}{N}\Sigma_{i=1}^{N}(R_i - R_{avg})^3}{\sigma^3} \tag{6}$$

where N is the total number of grains, R_i is the radius of grain i calculated from the cubic root of the grain volume, i.e. assuming all grains to be a cube, R_{avg} is the mean radius and σ is the standard

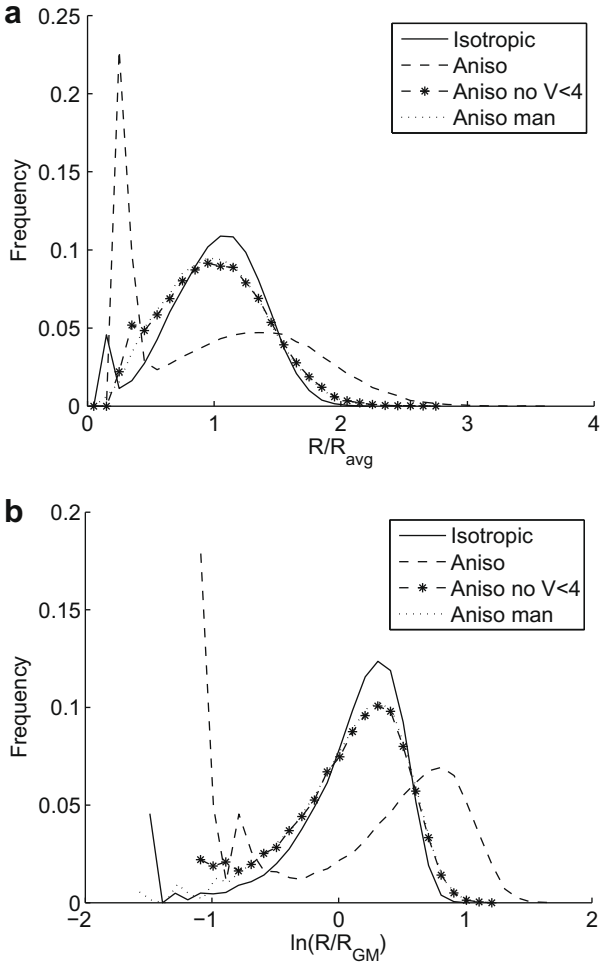

Fig. 6. Graphs comparing a fully isotropic system, Case 1, a fully anisotropic system, Case 7, a fully anisotropic system with all grains with a volume of $V \leqslant 3$ removed and a fully anisotropic system where the small grains have been manually "removed" by smoothing. (a) The size distributions on a linear scale. (b) The size distributions on a logarithmic scale.

Table 2
The calculated skewness for the original distribution (including all grains).

Case	Type of GBE and mob	Skewness of linear-scale distribution	Skewness of log-scale distribution	Standard deviation (σ)
1	Full isotropy, mob = 1	−0.28	−1.56	0.37
2	Isotropic GBE, step mob	−0.27	−1.47	0.39
3	RS GBE, isotropic mob	−0.14	−1.34	0.42
4	RS GBE and step mob	−0.17	−1.18	0.44
5	Aniso GBE, step mob	0.25	−0.81	0.55
6	RS GBE, aniso mob	0.26	−0.47	0.60
7	Full (original) anisotropy	0.42	−0.27	0.66

Table 3
The calculated skewness for manually corrected distributions removing the peak at small grain sizes by smoothing.

Case	Type of GBE and mob	Skewness of linear-scale distribution	Skewness of log-scale distribution	Standard deviation (σ)
1	Full isotropy, mob = 1	−0.09	−1.18	0.32
2	Isotropic GBE, step mob	−0.04	−1.13	0.32
3	RS GBE, isotropic mob	−0.14	−1.03	0.33
4	RS GBE and step mob	0.04	−1.08	0.33
5	Aniso GBE, step mob	0.51	−0.92	0.38
6	RS GBE, aniso mob	0.17	−0.92	0.39
7	Full (original) anisotropy	0.23	−0.87	0.39

deviation. An analogous expression applies for the skewness of a distribution on a log-scale, where R_i in Eq. (6) is replaced with $\ln(R_i)$ and R_{avg} is replaced with $\ln(R_{GM})$.

If the distribution has a more pronounced (longer) tail on the left-hand side than on the right-hand side, it is denoted negatively skewed or left-skewed, while if it has a more pronounced tail on the right-hand side than on the left side, it is named positively skewed or right-skewed. The closer the skewness is to zero the closer the distribution is (at least in principle) to a symmetrical or normal or log-normal distribution, respectively, depending on the representation.

Tables 2 and 3 give the calculated skewness in the various grain size distributions. In Table 2 the skewness is calculated for the original distribution while in Table 3 the calculations are based on the distributions which, as earlier mentioned, have been manipulated to give a "best fit" for the small grains.

It is seen in Fig. 6 that removing all small grains dramatically change the shape of the anisotropic grain size distribution, and as seen it is much closer to the size distribution for the isotropic case than to the original one for the anisotropic case. However, comparing now the calculated skewness in the isotropic distribution with the skewness in the fully anisotropic case, both for the cases with all the small grains present and for the cases where the distributions have been manually "corrected" for the small grains, see Tables 2 and 3, respectively, a tendency of a shift from a normal-like distribution towards a log-normal-like distribution is seen.

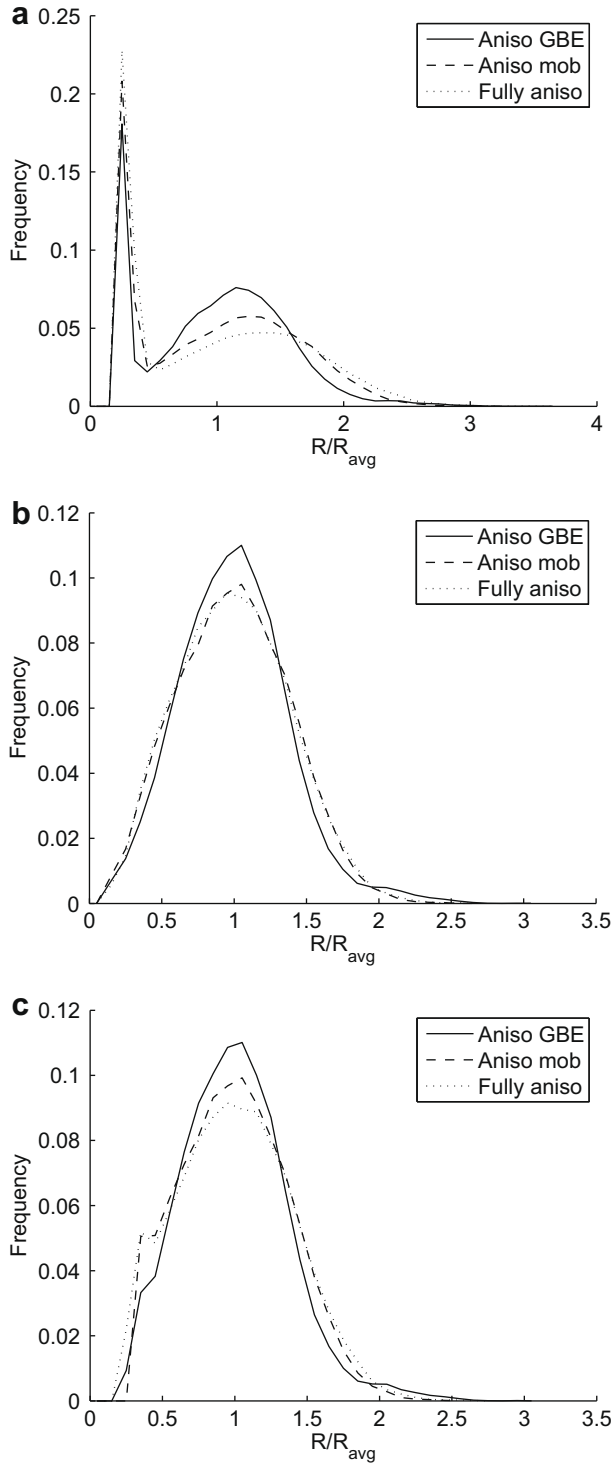

Fig. 7. Graphs comparing the grain size distributions for simulations with anisotropic grain boundary energy and step mobility, Case 5, anisotropic mobility and Read–Shockley grain boundary energy, Case 6, and a fully anisotropic system, Case 7. (a) The original grain size distributions. (b) The grain size distributions after a manual "correction" of the distributions. (c) The grain size distributions after removing all grains with $V \leqslant 3$ lattice sites.

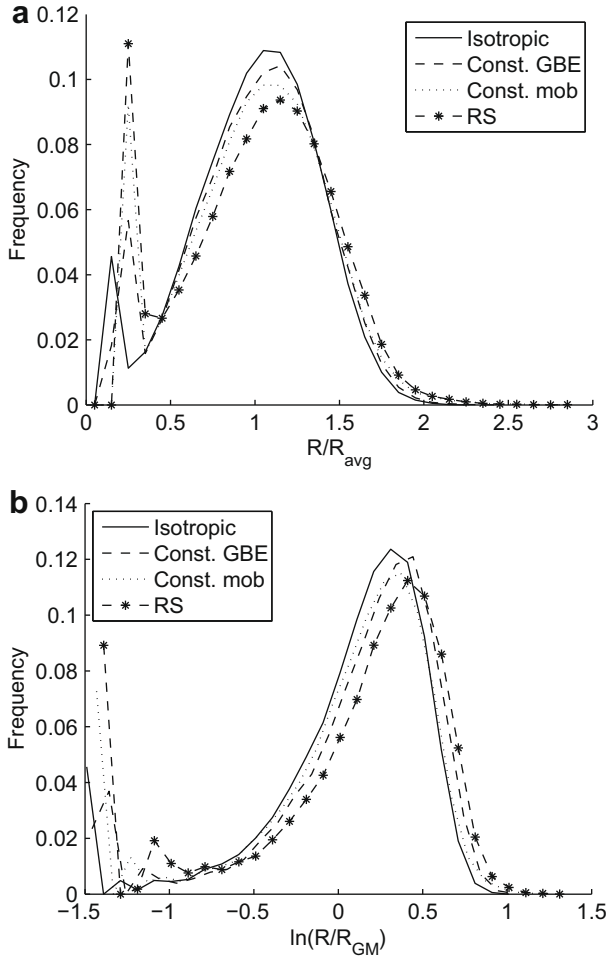

Fig. 8. Graphs comparing the (original; as simulated) grain size distributions for a fully isotropic system, Case 1, a system with constant grain boundary energy and a step mobility, Case 2, a system with constant mobility and a Read–Shockley grain boundary energy, Case 3, and a system with a RS grain boundary energy and a step mobility, Case 4. (a) The size distributions on a linear scale. (b) The size distributions on a logarithmic scale.

However, one should also be cautious with the skewness values, as they may be misleading due to the extra peaks at small grains. For example, for the fully anisotropic case, Case 7, in Table 2, the skewness for the log-scale distribution is calculated to have a value close to zero (−0.27), however, the peak for small grains greatly affect this calculation and the grain size distribution is in reality far from being close to log-normal.

Fig. 7 compares the grain size distribution for three particular cases; anisotropic GBE and a stepped mobility function (without CSLs), Case 5, anisotropic mobility and RS GBE, Case 6, and a fully anisotropic system, Case 7.

As we see, there are clear changes in the size distributions, where the original size distributions are shown in Fig. 7a. However, due to the large peaks for small grains, it is difficult to characterise and quantify the shape changes. To facilitate a direct comparison we have therefore also included the size distributions after manipulation using the two methods of removing the small grains introduced above. The resulting size distributions are shown in Fig. 7b and c, respectively.

When comparing Fig. 7b with c, it is seen that both approaches give quite similar results. However, as the method with a manually extrapolated distribution at small grains gives the smoothest curves and because of the small differences, only the manually cor-

Table 4
An overview of the different simulation cases including the calculated skewness in the corresponding grain size distributions.

Vol.% of particles	With nuclei	Time (MCS)	Skewness of linear-scale distribution	Skewness of log-scale distribution
0		100	0.24	−1.05
0		600	0.31	−1.30
0		800	0.37	−1.42
0	*X*	90	1.65	−0.58
0	*X*	200	−0.46	−2.02
0	*X*	300	−0.22	−1.99
1	*X*	100	1.73	−0.50
1	*X*	500	−0.12	−1.84
1	*X*	1000	0.12	−1.60
2	*X*	100	1.73	−0.51
2	*X*	600	−0.17	−1.92
2	*X*	2000	0.44	−1.27
5		100	0.20	−1.08
5		2000	0.79	−0.95
5		3000	0.91	−0.60
5		8×10^5	1.25	0.32
5	*X*	100	1.71	−0.57
5	*X*	1000	−0.15	−2.05
5	*X*	1×10^4	0.77	−1.11
5	*X*	1×10^5	4.65	−0.03
10	*X*	100	1.63	−0.68
10	*X*	1×10^4	0.08	−1.54
10	*X*	1×10^6	0.24	−0.52

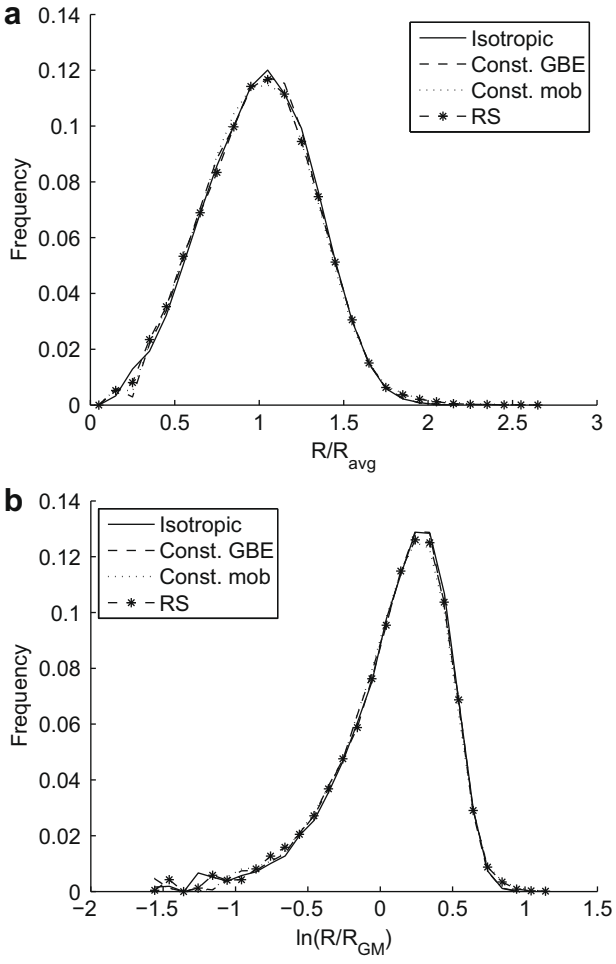

Fig. 9. Graphs comparing the grain size distribution for a fully isotropic system, Case 1, a system with constant grain boundary energy and step mobility, Case 2, a system with constant mobility and a Read–Shockley grain boundary energy, Case 3, and a system with Read–Shockley grain boundary energy and step mobility, Case 4. All distributions are manually smoothened for the small grains. (a) The size distributions on a linear scale. (b) The size distributions on a logarithmic scale.

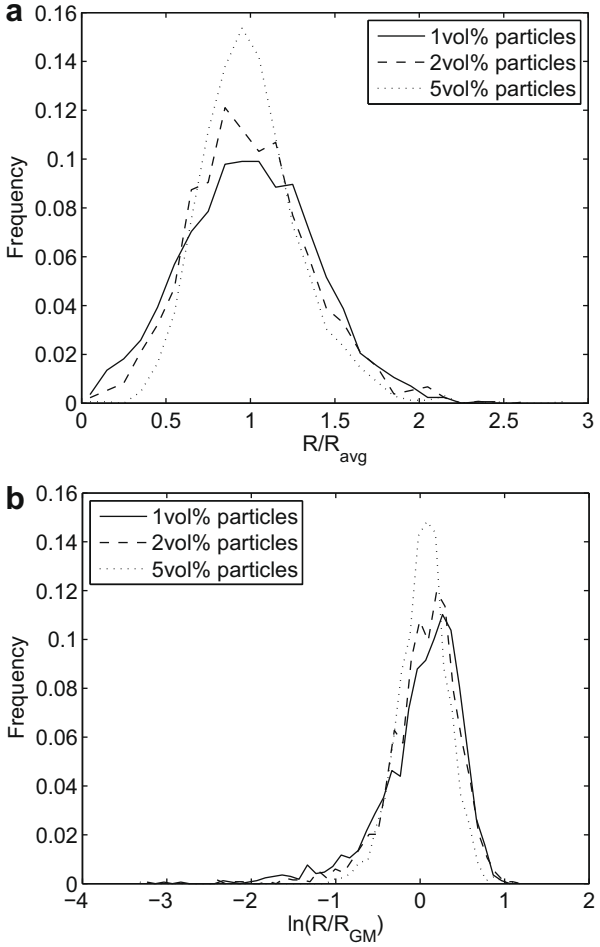

Fig. 10. The grain size distributions for the cases of 1 vol.%, 2 vol.% and 5 vol.% of particles. In all cases, initially 0.05 vol.% of nuclei were added. All cases show the distribution when approximately 1500 grains are left in the microstructure. (a) The size distributions on a linear scale. (b) The size distributions on a logarithmic scale.

rected distributions have been chosen for further considerations and calculations, cf. Table 3. If we compare the skewness values for these three cases (Cases 5–7), the values calculated for the original distributions, Table 2, indicate a small shift towards log-normality, e.g. γ_1 decreasing nominally from −0.81 to −0.27 for the log-scale distributions.

Turning to the skewness values, as calculated for the "corrected" size distributions, Table 3, which supposedly more directly reflect the real skewness (since the extra peak at small grains is removed), the indications are less clear, although the log-scale distributions still indicate a minor change consistent with a small shift in the direction of log-normality. However, the absolute values are still much higher than for the linear-scale distributions (e.g. −0.87 vs. 0.23 for Case 7). Fig. 7b shows that the main difference between these cases is that the anisotropic grain boundary energy case (Case 5) gives a slightly more narrow peak in the grain size distribution than the two other cases.

Figs. 8 and 9 illustrate the cases with the lowest anisotropy, Cases 1–4, respectively for the original and for the manually corrected grain size distributions. As seen in Tables 2 and 3 there are only small differences in skewness between these cases, although a very small increase in the skewness with increasing anisotropy is seen. This is consistent with the observation in Figs. 8a and 9a, where the right-hand tail increases slightly with increasing anisotropy, i.e. a small indication of a shift from a normal-like towards a log-normal-like distribution.

Considering the overall trend in Table 2, there is a shift from a left-skewed towards a right-skewed grain size distribution on the linear scale. The fully anisotropic case is still not completely symmetric on a log-scale, but the skewness value indicates that it is closer to a log-normal-like distribution than to a normal-like distribution. However, as mentioned earlier, as these cases have an artificially large fraction of small grains which affects the calculation of the skewness, these numbers can be misleading.

Nevertheless, also for the manually corrected cases, Table 3, which are believed to better represent true microstructures, the trend is the same, although less clear. The skewness of the log-scale distributions monotonically increases towards 0 with increasing anisotropy, from a value of −1.18 for the fully isotropic case to −0.87 for the fully anisotropic case.

4. Effect of particles on the grain size distribution

4.1. Simulation setup

In this part a parallel version of the standard 3D MC computer code, described in Section 2 [8,10], has been used to analyse the ef-

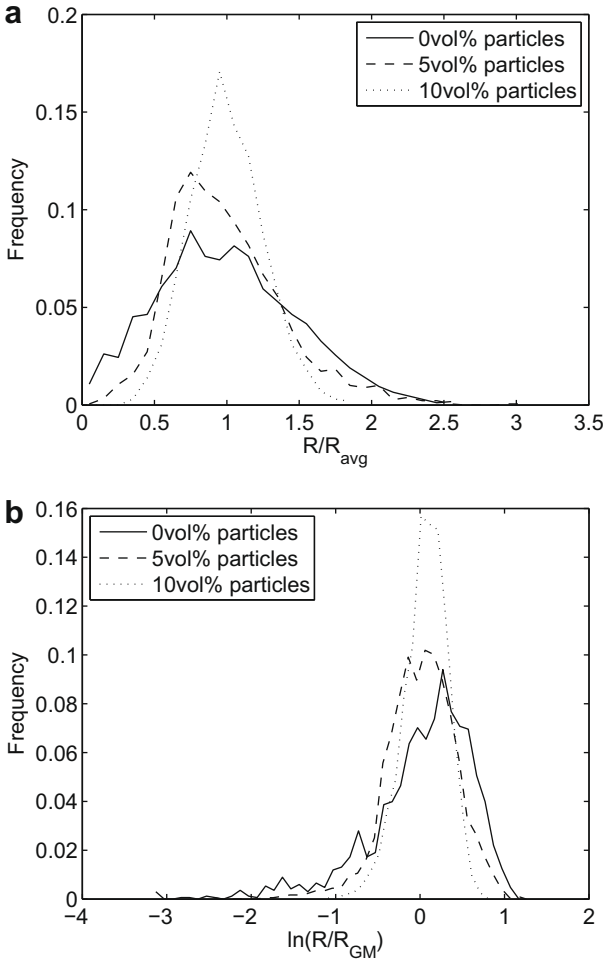

Fig. 11. The grain size distribution for the cases of 0 vol.%, 5 vol.% and 10 vol.% of particles. The two first cases correspond to grain growth only while in the latter case initially 0.05 vol.% of recrystallisation nuclei are added. The two first cases correspond to a situation where approximate 1700 grains are left in the microstructure while the latter case shows the distribution close to pinning. (a) The size distributions on a linear scale. (b) The size distributions on a logarithmic scale.

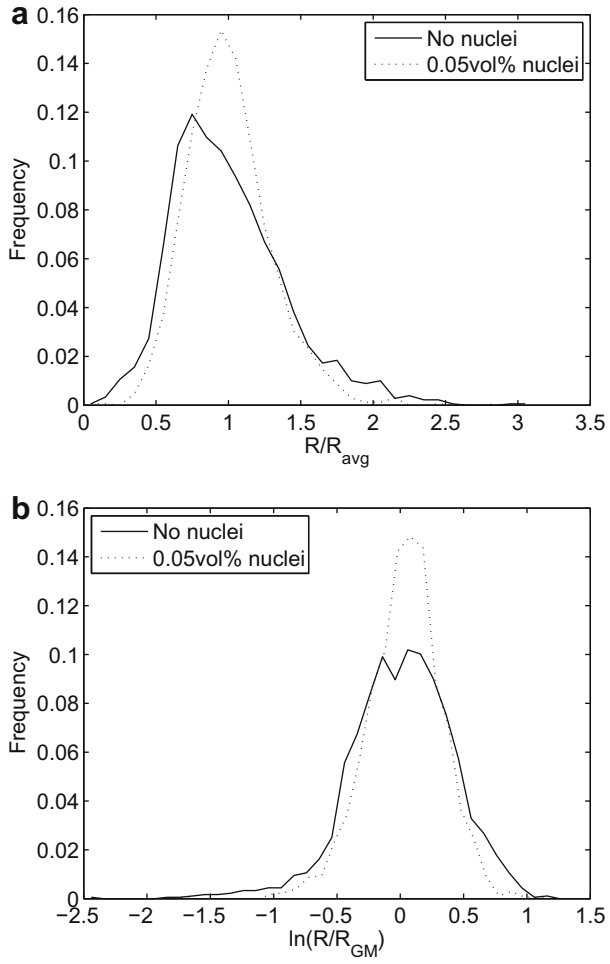

Fig. 12. The grain size distribution for a system with only grain growth and for a system with both recrystallisation and grain growth. Both cases have 5 vol.% of particles. The cases show the distributions when approximately 1700 grains are left in the microstructure. (a) The size distributions on a linear scale. (b) The size distributions on a logarithmic scale.

fects of particles on grain size distributions during grain growth only and during combined recrystallisation and grain growth simulations (provided by the courtesy of Dr. E. Holm, Sandia National Laboratories and Prof. Rollett, CMU, Pittsburgh, USA). This particular code was originally developed for grain growth and for running very large system sizes [28], which is necessary when including second phase particles [11], and lately also modified by Roberts [29] to start the simulations from a coarsened microstructure. The option of including recrystallisation has been implemented by the present authors.

These simulations are all run on an isotropic system, i.e. $\gamma(S_i, S_j) = 1.0$ and $M(S_i, S_j) = 1.0$, see Eq. (2). The system size is 400^3 lattice sites and initially each lattice site is given a random spin number between 1 and 10,000, i.e. each grain occupied on average one lattice site. This is a somewhat strange, artificial, initial microstructure. However, as long as the stored energy is scaled with the initial deformed grain size, in such a way that it is always energetically favourable for nuclei to grow, or just kept high (around 10 times the grain boundary energy if the average deformed grains is less than 5 times the nuclei size), the recrystallisation behaviour is barely affected. As for the serial code, periodic boundary conditions and a simulation "temperature" of $kT = 0.9$ are used. If the possibility of recrystallisation is added, the nuclei constitute a vol.% of 0.05 at time zero (site saturated nucleation) and each nucleus occupies one lattice site. Different fractions of randomly distributed particles have been added, ranging from 0% to 10%, and each particle occupy 3^3 lattice sites.

Simulations were run both with and without recrystallisation prior to grain growth, to see what effect this had on the grain size distribution and its evolution.

4.2. Results and discussion

Table 4 gives an overview of the different simulation cases with some key parameters for the various cases, including calculated values for the skewness both for the linear-scale distributions and the log-scale distributions.

Before turning to the actual results, a few comments are needed. When comparing coarsened microstructures, in this context defined to be a microstructure with around 1700 grains, for the case with and without recrystallisation prior to grain growth, the differences in grain size distributions are very small, but there are a few other differences. The main difference relates to the time it takes to get to this coarsened state – for the simulations with recrystallisation this takes a considerably longer time, i.e. with 5 vol.% of particles, the simulation including recrystallisation takes 3 times longer to reach a microstructure with approximate 1700 grains than the simulation without recrystallisation. Simulations with and without recrystallisation are presented in the same figures, but it is pointed out that the comparisons are not made at

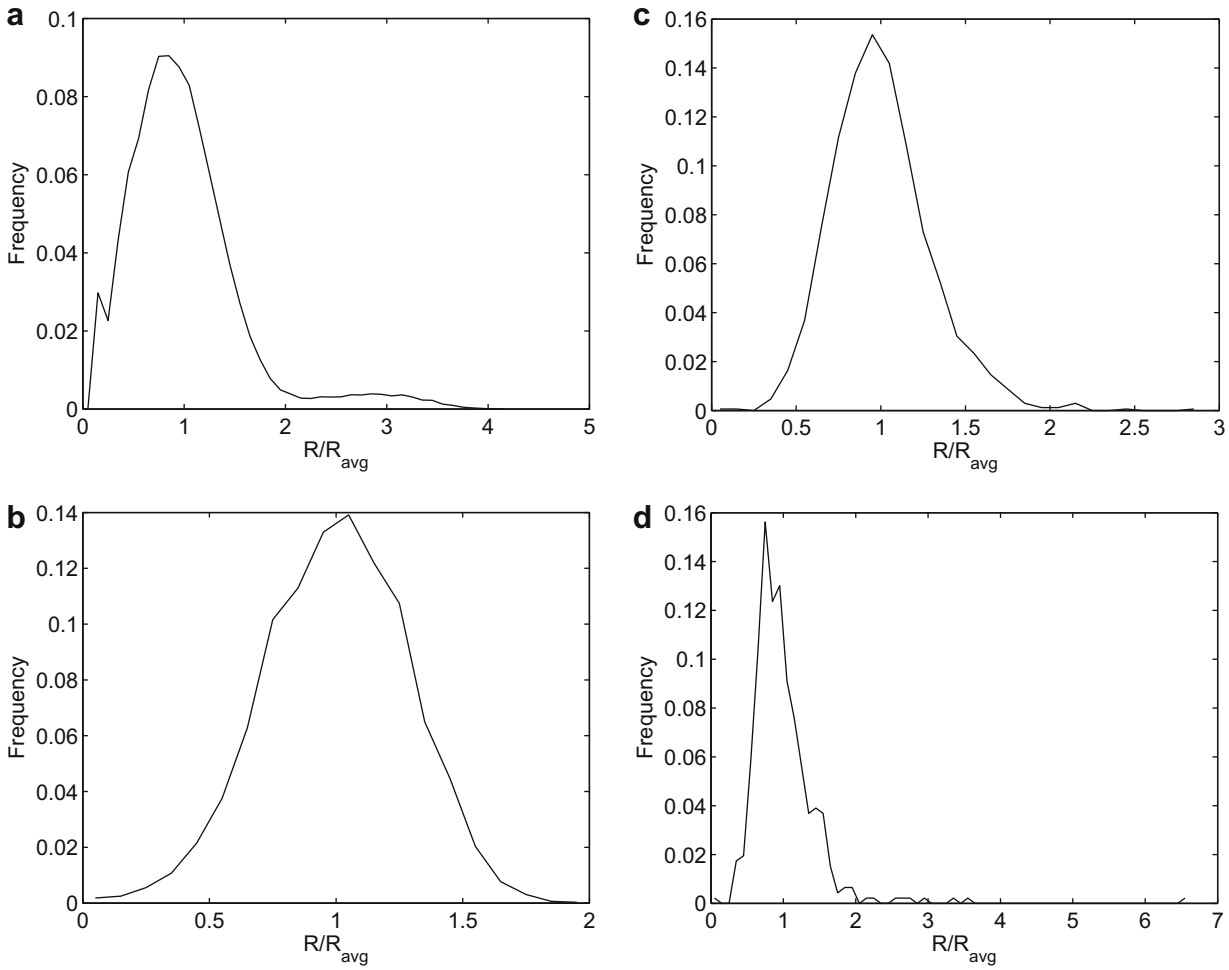

Fig. 13. Simulation with 5 vol.% of particles and initially 0.05 vol.% of recrystallisation nuclei. The different graphs (a–d) illustrate the evolution of the grain size distribution with time. (a) After 100 MSC. (b) After 1000 MSC. (c) After 10^4 MSC. (d) After 10^5 MSC.

the same times, instead they are made when the number of grains are approximately the same.

We start the discussion by considering the effect of an increasing amount of particles on severely coarsened microstructures, see Fig. 10. As observed in Fig. 10b, the grain size distribution changes from a left-skewed to a more log-normal-like distribution, at the same time as there is a sharpening of the distribution. Comparing the corresponding skewness values in Table 4, the same trend is observed. When increasing the particle fraction from 1 to 2 to 5 vol.%, the skewness of the log-scale distributions increases from -1.60 to respectively, -1.27 and -0.03. All grain size distributions in these cases are calculated when the microstructure consists of approximately 1500 grains. However, since the Zener limiting grain size is inversely proportional to the volume fraction of particles, the case of 5 vol.% of particles is closer to the pinned grain size than the two other cases. It is speculated that if also the cases with lower volume fractions of particles had been run to longer times, i.e. closer to the Zener limiting grain size, also these grain size distributions would have had a closer to log-normal shape. However, more simulations giving better statistics are needed to possibly confirm this speculation.

The lower the particle fraction, the faster the microstructure is coarsened, and since the distributions are compared when the cases have approximately the same number of grains, the sharpening seen in Fig. 10 might be an effect of the increased simulation time needed to reach the same coarsened microstructure.

The same apparent shift towards a log-normal distribution can also be seen in Fig. 11, which compares cases with 0, 5 and 10 vol.% of particles. For 0 vol.% of particles the skewness on log-scale is -1.42 while it is 0.32 in the case of 5 vol.% of particles. However, for the case of 10 vol.% of particles the skewness is decreased to -0.52. This may be because of the high particle fraction this microstructure is pinned before it reaches a near log-normal grain size distribution, and it never actually reaches around 1500 grains, which is used for comparison between the other cases. After 10^6 MCS, 2677 grains are still present in the microstructure.

It is pointed out that the cases discussed in relation to Fig. 11 include cases with grain growth only, while the latter case (the one with 10 vol.% of particles) refers to grain growth preceded by recrystallisation in the same simulation. To explicitly explore the effect of including recrystallisation, a direct comparison between a case of only grain growth and a case of grain growth following recrystallisation, both with 5 vol.% of particles, is also made, see Fig. 12. It is here clearly seen that for both cases the coarsened microstructures are close to having a log-normal distribution (the skewness on log-scale $\gamma_1 = 0.32$ with only grain growth and for the case with grain growth following recrystallisation $\gamma_1 = -0.03$), although the latter case, with recrystallisation, has a much sharper distribution. Both cases refer to approximately 1700 grains, but for the grain growth case this is reached after 3000 MCS, while for the recrystallisation plus grain growth case this is not reached until after 10,000 MCS, i.e. it seems that the dis-

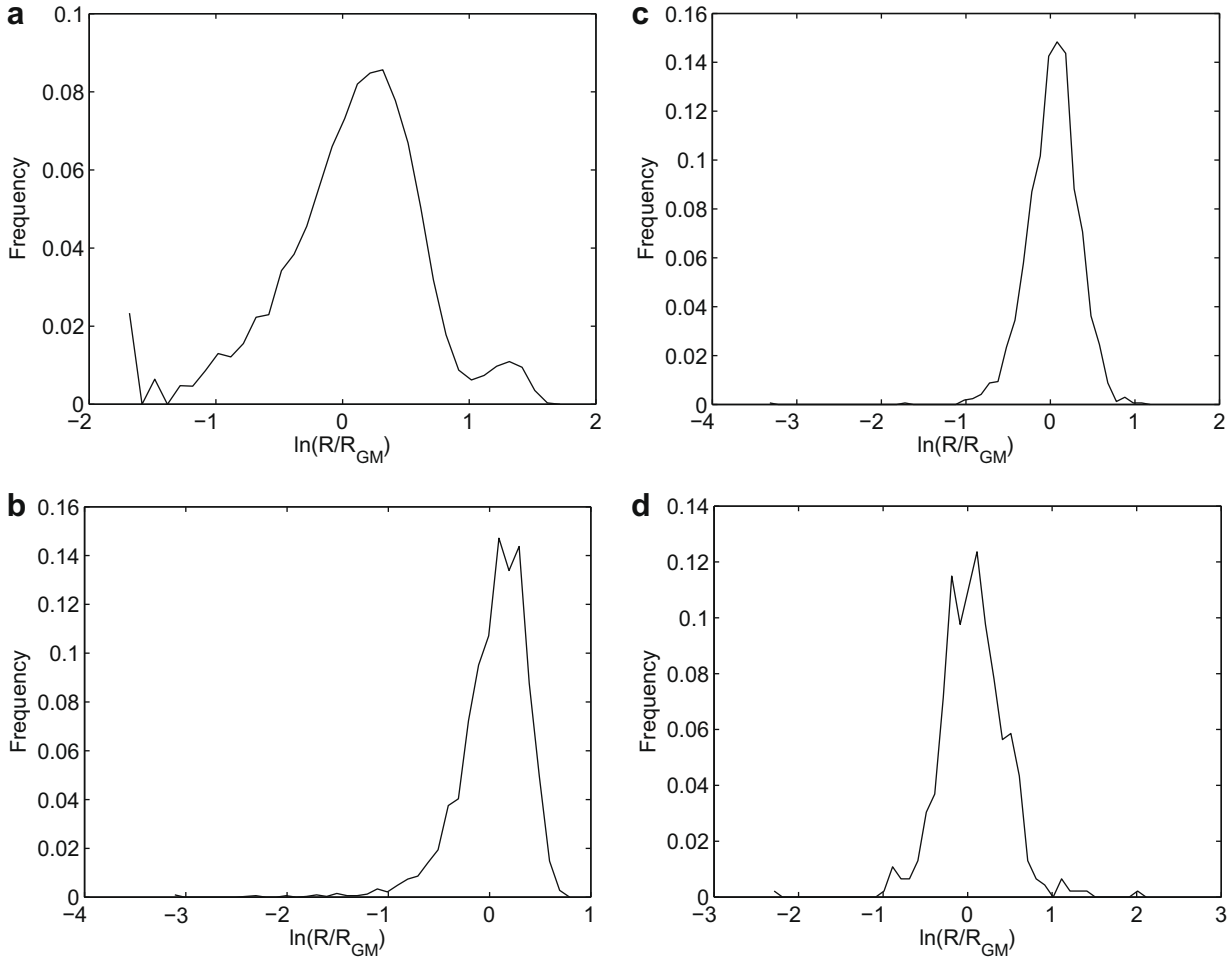

Fig. 14. Simulation with 5 vol.% of particles and initially 0.05 vol.% of recrystallisation nuclei. The different graphs (a–d) illustrate the evolution of the grain size distribution on logarithmic scale with time. (a) After 100 MSC. (b) After 100 MSC. (c) After 10^4 MSC. (d) After 10^5 MSC.

tribution is sharpened with time, just as in the distributions in Fig. 11.

Also the case without particles, has been run with and without preceding recrystallisation, (see Table 4). Initially the case with 0 vol.% of particles with and without recrystallisation behaves in the same way as the simulations with 5 vol.% of nuclei, i.e. after approximately 100 MCS the case without recrystallisation has a close to normal distribution (skewness on a linear scale equal to 0.24), while the case with recrystallisation has a distribution which is closer to log-normal (skewness on log-scale equal to −0.58). Then after coarsening the case without recrystallisation continues to have a near normal distribution (skewness around 0.3), while the case with recrystallisation has moved from a log-normal towards a normal distribution (skewness of −0.22 on a linear scale after 300 MCS). Again, the case with recrystallisation coarsens faster than the case without recrystallisation, which is the reason for the different simulation times in the two cases that are compared.

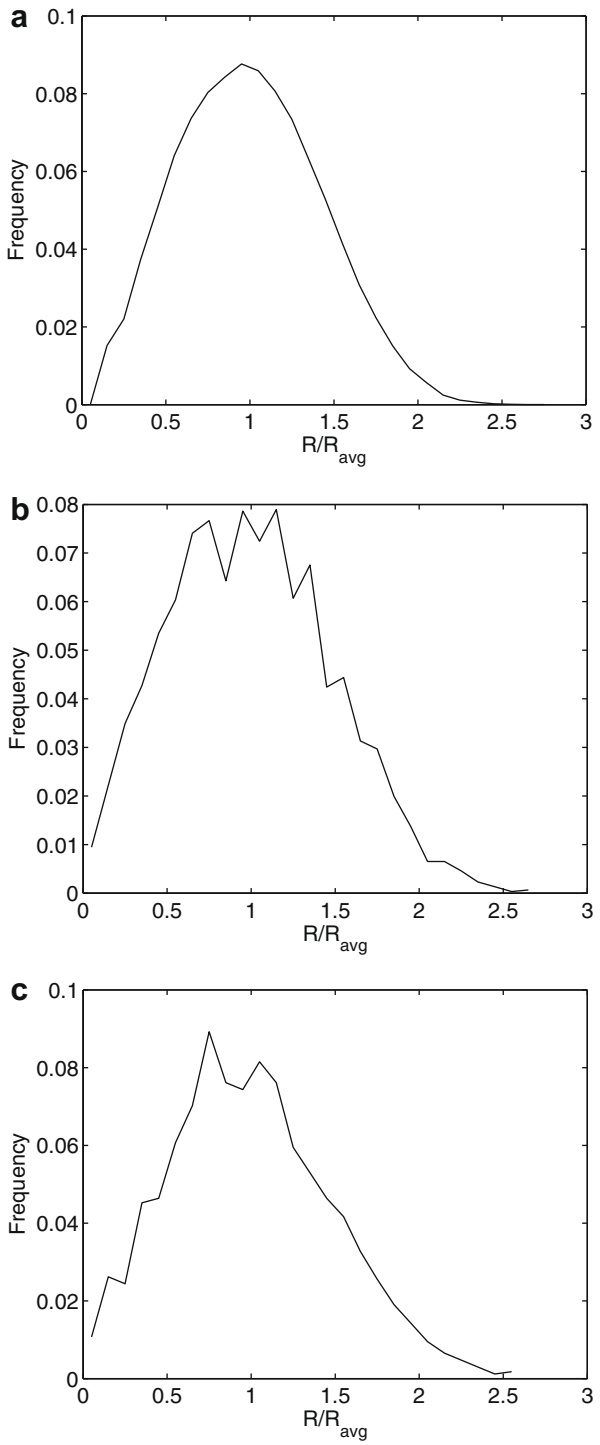

Fig. 15. Simulation of ordinary grain growth, i.e. without particles and without recrystallisation nuclei. The different graphs (a–d) illustrate the evolution of the grain size distribution with time. (a) After 100 MSC. (b) After 600 MSC. (c) After 800 MSC.

To get a better idea on how the size distributions actually develop with time, Figs. 13 and 14 show the time evolution of the size distribution on a linear and a logarithmic scale, respectively, for a simulation with 5 vol.% of particles where initially 0.05 vol.% of recrystallisation nuclei were added. After 100 MCS a characteristic small second peak is seen in the right end of the size distribution. This peak is not seen in the simulation cases without recrystallisation, i.e. its appearance has to be related to the recrystallisation nuclei and the growth of recrystallised grains in the microstructure. After 100 MCS already approximately 50% of the microstructure is recrystallised, so this seems reasonable.

There seem to be three stages in the time evolution of the grain size distributions in microstructures with recrystallisation and particles present. In the beginning there are two peaks (Fig. 13a), a situation which has some similarities to a bimodal distribution due to abnormal grain growth [24], where the recrystallised grains give rise to the second, small peak, i.e. a kind of abnormal grains. When the microstructure is 100% recrystallised, the distribution has shifted to a close to normal distribution (Fig. 13b), before it finally moves towards a log-normal distribution (Fig. 14c and d). These qualitative observations, including the different stages, are confirmed by the corresponding skewness values in Table 4, for all cases including both recrystallisation and particles. As an example, consider the case with 5 vol.% of particles and nuclei present, see Table 4. After 100 MCS the log-scale skewness is −0.57, after 1000 MCS this is lowered to −2.05, i.e. a higher absolute value, before it after 10^5 MCS has increased to a value of −0.03 (i.e. very close to a log-normal-like distribution). The latter case refers to really severe coarsening where the number of grains has decreased to 461. The same severe coarsening is also seen in the case with 5 vol.% of particles and no recrystallisation, where the microstructure after 8×10^5 MCS consists of only 273 grains.

The only exception from the three stages is the case with just grain growth, where the calculated skewness, both on linear and log-scale, monotonically increases. That is, the second stage, where the distribution moves towards a normal-like distribution, is not seen.

As a reference the corresponding development in the grain size distribution for a simulation of ordinary grain growth, i.e. no second phase particles, is seen in Fig. 15, presented on a logarithmic scale. The times presented in these figures are lower because no particles are retarding the growth, and the microstructure evolves much faster. It is clearly seen that the distribution hardly changes with time, which is also confirmed by the skewness values in Table 4.

5. Discussion and conclusions

The present paper has considered 3D grain size distributions and how they evolve during and after recrystallisation and grain growth. Two particular cases have been studied: (i) the effects of anisotropy in grain boundary energy and boundary mobility (dependent on misorientation) on grain size distributions after recrystallisation and (ii) the effects of second phase particles on the size distributions after both recrystallisation and grain growth.

Concerning the effect of anisotropy, the present 3D MC simulations have shown that anisotropy has a strong effect on the size

distributions of grains after recrystallisation, however, mainly in terms of a large and increasing fraction of small grains with increasing anisotropy. The large fraction of small grains, showing up as an extra peak at small grains in the size distributions, complicates a simple characterisation of the distribution shape and also a straight forward comparison of the size distributions following recrystallisation simulations with varying degree of anisotropy (in grain boundary energy and mobility). To facilitate a direct comparison, two different ways of dealing with/removing the small grains have been considered. After "correcting" for the unrealistic large number of small grains the differences between the different cases become quite small and it is difficult to characterise the shape changes from visual inspection alone.

As a more quantitative measure the skewness, γ_1, was introduced and calculated for all the size distributions, both the original ones and the manually corrected ones. The evaluation of skewness in the original grain size distribution indicates a shift from a normal to a log-normal distribution, i.e. a decreasing absolute value in skewness (of the log-scale distributions) approaching zero for the fully anisotropic case (indicating a near symmetric log-normal shape). However, as most of the original size distributions (those with anisotropy) contain a large amount of small grains, the calculated skewness in these cases may be misleading. Nevertheless, the same trend is also seen for the manually corrected cases, although the differences between the skewness values in the isotropic and anisotropic cases are quite small (i.e. -1.18 and -0.87, respectively). Moreover, when only considering the nominal values, the skewness values actually indicate a shape closer to a normal ($\gamma_1 = -0.23$) than a log-normal ($\gamma_1 = -0.87$) grain size distribution.

The present simulations have been performed with a simulation temperature of $kT = 0.9$, in accordance with Brahme [16]. However, to test the sensitivity to this parameter, a sub-set of simulations has been carried out with higher and lower lattice temperatures to see to which extent this influences the general results. Fig. 16 shows the grain size distributions (as simulated) for the case of Read–Shockley grain boundary energy (GBE) and a step mobility (Case 4) resulting from simulations for values of $kT = 0.5$, 0.9, 1.2 and 1.5. As demonstrated only minor changes are observed and

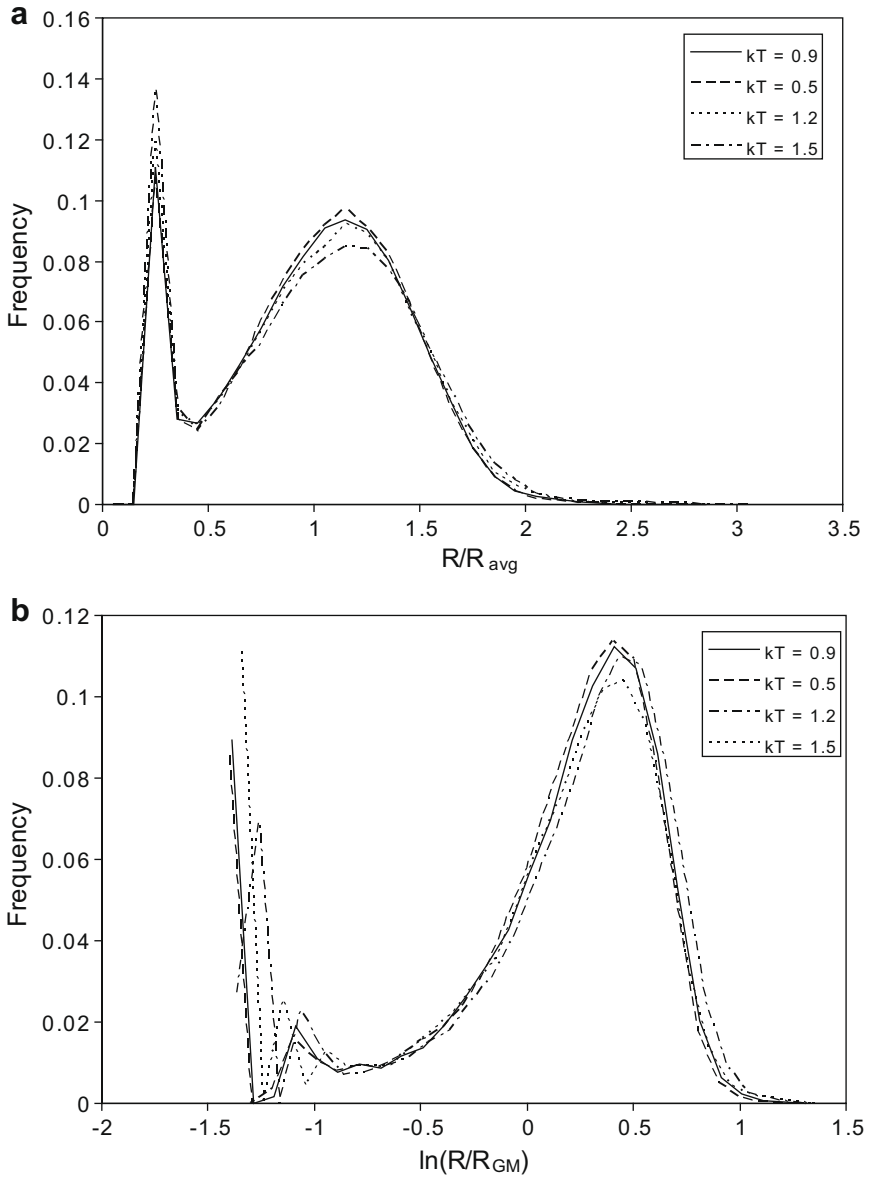

Fig. 16. Grain size distributions for the case with a Read–Shockley grain boundary energy and step mobility (Case 4) comparing different simulations temperatures $kT = 0.5$, 0.9, 1.2, 1.5. (a) The size distributions on a linear scale. (b) The size distributions on a logarithmic scale.

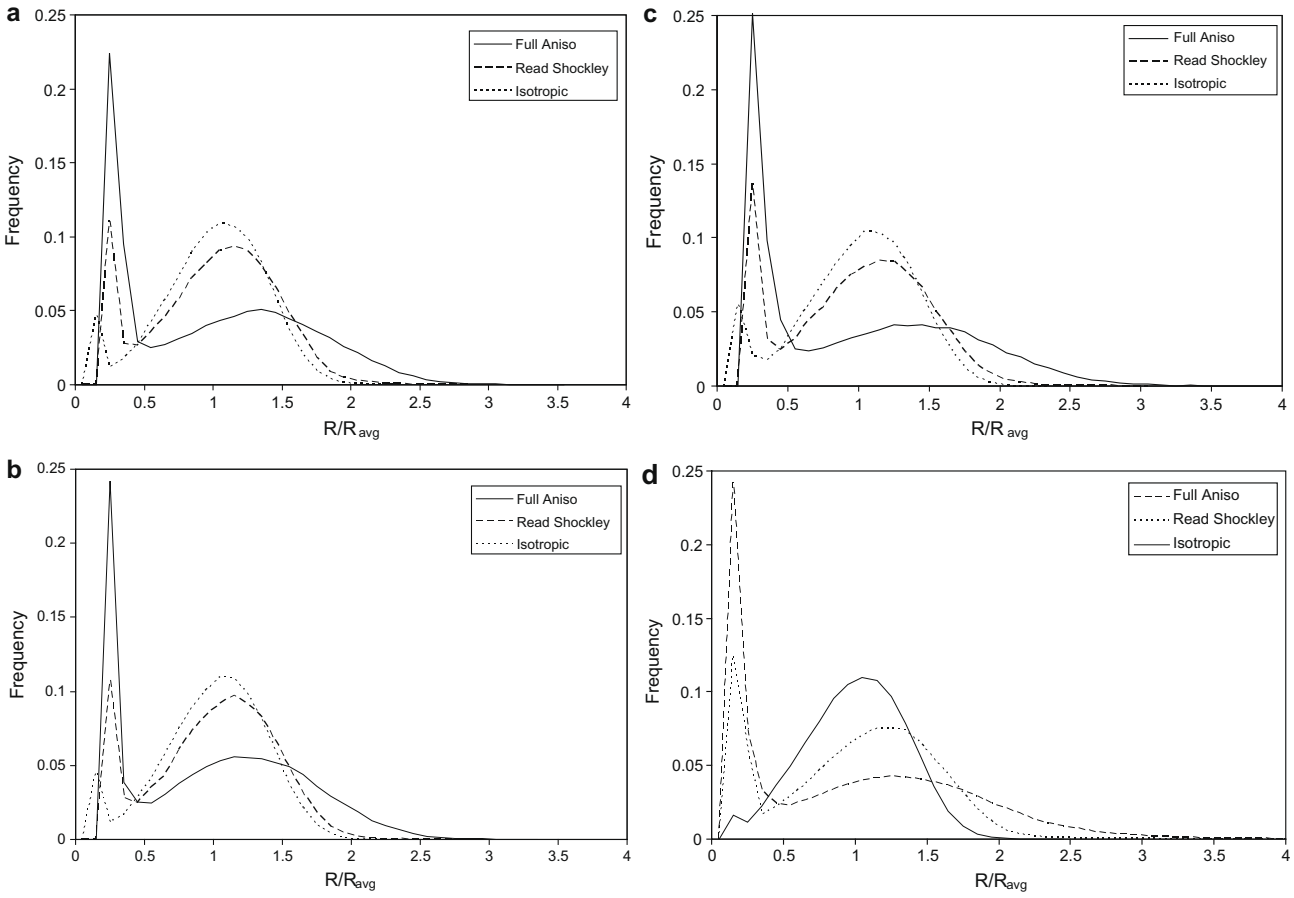

Fig. 17. Graphs comparing the grain size distributions (linear scale) for a fully isotropic system, Case 1, a system with Read–Shockley grain boundary energy and step mobility, Case 4, and a fully anisotropic system (including CSLs), Case 7. (a) $kT = 0.9$, (b) $kT = 0.5$, (c) $kT = 1.5$. The grain size distributions in a–c all correspond to a system size $100 \times 100 \times 100$. (d) The grain size distributions for Case 1, Case 4 and Case 7, and $kT = 0.9$, for a system size of $200 \times 200 \times 200$.

in particular the size distributions for the three lower simulation temperatures are very close, and for the $kT = 0.9$ case the curve lies in between the two others. The same result (not included) has also been confirmed for the fully isotropic case (Case 1) and the fully anisotropic case (Case 7). Moreover, as demonstrated in Fig. 17, the same variations with the degree of anisotropy are obtained, exemplified by comparing the size distributions (on a linear scale) following a fully isotropic case (Case 1), Read–Shockley GBE and step mobility (Case 4) and a fully anisotropic case (Case 7), for $kT = 0.5$, 0.9, and 1.5 (Fig. 17a–c). Finally, a sub-set of simulations has also been run with a larger system size, i.e. with a 200^3 lattice. Again, although there are some small differences, the general trends in the results (in view of anisotropy) are the same, as shown in Fig. 17d. In summary, these results clearly indicate that the present results are not critically dependent on the simulation temperature or the system size and that the general effects of anisotropy are real and representative, and not an artefact of the simulation temperature or limited system size.

In the second part of the paper, a fully isotropic 3D MC model (parallel code) was used to study the effect of particles on grain size distributions after both recrystallisation and grain growth. It must be emphasised that for these cases only one simulation has been run for each case, as these simulations are quite demanding in terms of computer power and storage. They have all been run on a high performance computer facility where we had limited amount of computational time. However, the simulations are run on a very large MC system (64 million lattice sites) and the grain size distributions generally are calculated from more than 1000 grains (except for two cases; the cases with 5 vol.% of particles (with and without recrystallisation nuclei), which are coarsened to even larger grains to see how the size distribution evolves with time up to very long simulations times).

The simulations have shown that for an increasing volume fraction of particles the coarsened microstructures show a clear shift from a Gaussian distribution towards a log-normal distribution. This behaviour is observed both for cases with grain growth alone and for the cases with both recrystallisation (preceding grain growth) and coarsening. Considering the evolution of the size distributions with time it is also demonstrated that the tendency of log-normality becomes even clearer for severely coarsened microstructures. However, for very large volume fractions of particles, in our simulations the case with 10 vol.% of particles, the microstructure only approaches log-normality, but not as close as for the 5 vol.% particle case. In the 10 vol.% particle case, the large amount of particles seems to pin the microstructure before it reaches a close to log-normal grain size distribution. On the other hand, the simulations have also shown that coarsening in a grain structure without particles shows little or no shape changes during coarsening, i.e. an initial nearly Gaussian distribution remains so during coarsening. This is in accordance with previous simulation work [30] and most prevailing theories for normal grain growth [31–33], which predicts a steady state size distribution during normal grain growth.

As a final remark, it can be concluded that the apparent universality of near log-normal size distributions of grains after recrystallisation and grain growth is still kind of a puzzle, however, the

present simulations have clearly shown that both anisotropy (in grain boundary energies and mobilities) has an influence and, even more so, second phase particles, which clearly drive the size distributions towards log-normality.

Acknowledgements

A. Brahme, C. Roberts and A.D. Rollett, Dept. of Materials Science and Engineering, Carnegie Mellon University, PA, USA are gratefully acknowledged for providing the MC software codes used in this work, and for help and stimulating discussions during the work. Thanks also to NOTUR, the Norwegian Metacentre for Computational Science for providing free CPU time at their supercomputers and to the NOTUR support group at NTNU for help and guidance with the implementation and debugging of the parallel MC code.

References

[1] I.M. Lifshitz, V.V. Slyozov, J. Phys. Chem. Solids 19 (1961) 35.
[2] C. Wagner, Z. Elektrochem. 65 (1961) 581.
[3] O.R. Myhr, Ø. Grong, Acta Mater. 48 (2000) 1605.
[4] J. Friis, B. Holmedal, Ø. Ryen, E. Nes, O.R. Myhr, Ø. Grong, T. Furu, K. Marthinsen, Mater. Sci. Forum 519–521 (2006) 1901.
[5] K. Marthinsen, O. Lohne, E. Nes, Acta Metall. 37 (1989) 135.
[6] K. Marthinsen, J.M. Fridy, T.N. Rouns, K.B. Lippert, E. Nes, Scripta Mater. 39 (1998) 1177.
[7] T. Furu, K. Marthinsen, E. Nes, Mater. Sci. Technol. 6 (1990) 1093.
[8] A.D. Rollett, Prog. Mater. Sci. 42 (1997) 79.
[9] M. Miodownik, J. Light Met. 2 (2002) 125.
[10] A.D. Rollett, P. Manohar, in: D. Raabe, F. Roters, F. Barlat, L.-Q. Chen (Eds.), Continuum Scale Simulation of Engineering Materials, Wiley-VCH, Weinheim, 2004, pp. 77–114.
[11] M. Miodownik, E.A. Holm, G.N. Hassold, Scripta Mater. 42 (2000) 1173.
[12] E. Fjeldberg, K. Marthinsen, in: J. Hirsch, B. Skrotzki, G. Gottstein (Eds.), Proceedings of the 11th International Conference on Aluminium Alloys, Wiley-VCH, Weinheim, 2008, pp. 1156–1162.
[13] G.S. Grest, D.J. Srlolovitz, M.P. Anderson, Acta Metall. 33 (1985) 509.
[14] A.D. Rollett, D.J. Srlolovitz, M.P. Anderson, Acta Metall. 37 (1989) 1227.
[15] E.A. Holm, G.N. Hassold, M.A. Miodownik, Acta Mater. 49 (2001) 2981.
[16] A.P. Brahme, Modelling Microstructure Evolution during Recrystallization. Ph.D. Thesis, Carnegie Mellon University, 2005.
[17] A. Brahme, J. Fridy, H. Weiland, A.D. Rollett, Modell. Simul. Mater. Sci. Eng. 17 (1) (2009) 015005.
[18] M.A. Alvi, S. Cheong, H. Weiland, A.D. Rollett, Acta Mater. 56 (2008) 3098.
[19] G.N. Hassold, E.A. Holm, Comput. Phys. 7 (1993) 97.
[20] A.P. Brahme, M.H. Alvi, D. Saylor, J. Fridy, A.D. Rollett, Scripta Mater. 55 (2006) 75.
[21] K. Marthinsen, S. Abtahi, K. Sjølstad, B. Holmedal, E. Nes, A. Johansen, J.A. Saeter, T. Furu, O. Engler, Z.J. Lok, J. Talamantes-Silva, C. Allen, C. Liu, Aluminium 80 (2004) 729.
[22] M. Miodownik, A.W. Godfrey, E.A. Holm, D.A. Hughes, Acta Mater. 49 (1999) 2661.
[23] O. Engler, Textures Microstruct. 32 (1999) 197.
[24] F.J. Humphreys, M. Hatherly, Recrystallization and Related Annealing Phenomena, second ed., Pergamon, Elsevier, Amsterdam, 2004.
[25] V. Marx, F.R. Reher, G. Gottstein, Acta Mater. 47 (1999) 1219.
[26] E. Fjeldberg, K. Marthinsen, On the recrystallisation kinetics of 3D Pott Monte Carlo simulations, ReX&GG IV, Sheffield, UK, 2010. submitted for publication.
[27] J.F. Kenney, E.S. Keeping, Mathematics of Statistics, Part 1, third ed., Van Nostrand, 1962.
[28] S.A. Wright, T.P. Plimpton, T.P. Swiler, R.M. Fye, M.F. Young, E.A. Holm, Technical Report 97-1925, SANDIA, August 1997.
[29] C. Roberts, Grain Growth and the Zener Pinning Phenomenon: A Computational and Experimental Investigation. Ph.D. Thesis, Carnegie Mellon University, 2007.
[30] C. Maurice, in: G. Gottstein, D.A. Molodov (Eds.), Recrystallization and Grain Growth, Springer-Verlag, Berlin, 2001, pp. 123–134.
[31] O. Hunderi, N. Ryum, J. Mater. Sci. 15 (1980) 1104.
[32] H.V. Atkinson, Acta Metall. 36 (1988) 469.
[33] W.W. Mullins, Acta Mater. 46 (1998) 6219.